

# COMPUTED TOMOGRAPHIC IMAGING OF THE NORMAL IMMATURE CALIFORNIA SEA LION HEAD (*ZALOPHUS CALIFORNIANUS*)

SOPHIE E. DENNISON, TOBIAS SCHWARZ

Different computed tomography (CT) protocols were tested to optimize imaging of the head of the California sea lion. Transverse mode images were superior to helical mode images. Bone structures were best imaged using 1 mm slice width combined with a high-frequency image reconstruction algorithm and best viewed using a wide window setting. Soft tissue structures were generally difficult to differentiate with the exception of the orbital region, which was best imaged using 2 mm slice width combined with a medium-frequency image reconstruction algorithm and best viewed using a narrow window setting. Anatomic features specific to the California sea lion were identified on CT images and were consistent with previously published data. These included absence of the lacrimal bone, nasolacrimal ducts, and paranasal sinuses. Upon qualitative assessment of the orbit and nasal cavity, there was a triangular-shaped interorbital nasal cavity on transverse images, and extensive, highly convoluted ethmoid turbinates. The permanent dental formula was identical to previous reports. In conclusion, we provide a detailed description of the anatomy of the immature California sea lion head and a definition of two imaging protocols. *Veterinary Radiology & Ultrasound, Vol. 49, No. 6, 2008, pp 557–563.*

**Key words:** computed tomography, diagnostic imaging, marine mammal, pinniped, skull.

## Introduction

NORMAL COMPUTED TOMOGRAPHY (CT) anatomic references of the head have been produced for the dog, horse, llama, and neonatal bottlenose dolphin (*Tursiops truncatus*).<sup>1–5</sup> Currently, the only published CT data in California sea lions (*Zalophus californianus*) is limited to the diagnosis of a nasal tumor.<sup>6</sup> Neoplasia, dental disease, and trauma have been observed in the head region of captive sea lions. In addition, free-ranging animals treated in rehabilitation centers frequently have neurologic signs or other conditions affecting the head.<sup>7–9</sup> In one study, 61% of all sea lion gunshot injuries, and the majority of entanglements, were associated with the head.<sup>7</sup>

Knowledge of detailed species-specific anatomic features facilitates characterization of lesions and permits accurate diagnosis of abnormalities within a region of interest. Knowledge of appropriate technical protocols for a study permits optimization of the image acquisition. Our aim was to describe a CT protocol and the normal CT anatomy of the immature California sea lion for use as a baseline reference.

## Materials and Method

Two fresh-frozen California sea lion cadavers were shipped under permit issued by the National Marine Fisheries Service from The Marine Mammal Center in Sausalito, California to the University of Wisconsin–Madison and allowed to thaw completely before CT examination. The cadavers were from two 10-month-old California sea lion pups, one male and one female, which died during rehabilitation from malnutrition and pneumonia. Age assessment was based on knowledge of the species-specific reproductive cycle. Both cadavers were frozen within 24 h of death, but the exact time between death and freezing was unknown.

Each cadaver was in sternal recumbency and centered in the gantry using the laser guidance system. The head was elevated such that the hard palate was parallel to the table. The body was positioned as straight as possible and maintained in position using foam wedges. The pelvic flippers were extended behind the cadaver while the pectoral flippers were positioned with the palmar surface adjacent to the thoracic wall.

A single-detector-row helical CT scanner (HiSpeed LXI\*) was used. Various single-slice and helical modes, slice thicknesses and reconstruction algorithms were assessed. Once acquired, all images were reviewed using dedicated imaging software (eFilm version 2.1.2†) by one author (S.D.). Window width (WW) = 2500 HU and

From the Department of Surgical Sciences, School of Veterinary Medicine, University of Wisconsin–Madison, 2015 Linden Drive, Madison, WI 53706, USA.

Address correspondence and reprint requests to Dr. Sophie E. Dennison, at the above address. E-mail: dennison@svm.vetmed.wisc.edu

Received February 14, 2008; accepted for publication April 7, 2008.  
doi: 10.1111/j.1740-8261.2008.00421.x

\*General Electrics Medical Systems, Milwaukee, WI.

†Merge Healthcare, Milwaukee, WI.

window level (WL)=480 HU for images acquired with the high-frequency reconstruction algorithm and WW=350 HU and WL=90 HU with the medium-frequency reconstruction algorithm. Window width and level were then adjusted to optimize evaluation and identification of bone and soft tissue structures. A display field of view of 25 cm was used for all studies and multiplanar reconstructions were performed. Line drawings were created by manipulation of the individual CT images using ImageJ software (public download available at [www.rsb.info.nih.gov/ij/](http://www.rsb.info.nih.gov/ij/)). All bones were identified according to the official anatomic nomenclature with anglicized terminology where appropriate.<sup>10</sup>

Postmortem examination was performed by a board-certified pathologist. The skin and musculature covering the head were removed to evaluate the integrity of the skull, and the tympanic bullae were opened to evaluate for middle ear abnormalities. Histopathologic assessment was not performed.

### Results

Low numbers of small, 2–3 mm long, nasal mites (presumptive *Orthohalarachne attenuata*) were attached to and embedded within the nasopharyngeal mucosa of both sea lion cadavers. Degradation of the eyes resulted in detachment of the retina in all four eyes. A small volume of acellular free fluid was found in the ethmoid turbinates. No gross abnormalities of the turbinates were evident. There was no evidence of fluid in the middle ear. The tympanic membranes were not specifically identified. Evidence of verminous pneumonia (presumptive *Parafilaroides decorum*) in both cadavers resulted in lung lobe consolidation with multifocal tan colored granulomas approximately 1 mm in size and in the presence of small “hair-like” structures after scraping the cut pulmonary parenchymal surfaces. A diagnosis of death due to malnutrition with concurrent verminous pneumonia was concluded for both

cadavers. Paranasal sinuses, nasolacrimal ducts, and the lacrimal bones were not visible during dissection in agreement with previously published anatomic descriptions.<sup>11</sup>

A selection of images of the sea lion head is shown in Figs. 1–9. Minimal soft tissue differentiation was possible in the cadavers used in this study. The exception was the orbital cavity where the fibrous capsule of the eyeball (sclera and cornea), the vitreous body, aqueous humor, lens, retrobulbar fat, and extraocular muscles were distinguishable due to their different attenuation properties. For these structures, optimal tissue differentiation was achieved using the medium-frequency image reconstruction algorithm with WW=300 HU and WL=100 HU. Gas bubbles were identified within the calvarium in the region of the cavernous sinuses and within the periphery of the brain.

Excellent bone detail of the calvarial bones, temporomandibular joints, hyoid apparatus, ethmoid turbinates, teeth, and structures of the middle and inner ears was achieved using the high-frequency image reconstruction algorithm with additional moderate edge enhancement viewed with WW=2500 HU and WL=500 HU settings. High-resolution CT (transverse mode, 1 mm slice width) resulted in improved conspicuity of small inner ear structures and transverse images were superior to multiplanar reconstruction images for their identification. The meniscus of the temporomandibular joint was not identified in any imaging sequence.

The caudal aspect of the nasal cavity, nasopharynx, and cranial aspect of the trachea contained small amounts of fluid-attenuating material. Nasal fluid partially obliterated the ethmoid turbinates.

The orbital cavities were large, inducing an elongated, triangular-shaped interorbital nasal cavity in the transverse imaging plane. Extensive, finely divided, highly convoluted turbinates extended throughout the nasal cavity to the cribriform plate and frontal bone; however, individual conchae could not be identified. Paranasal sinuses, lacrimal

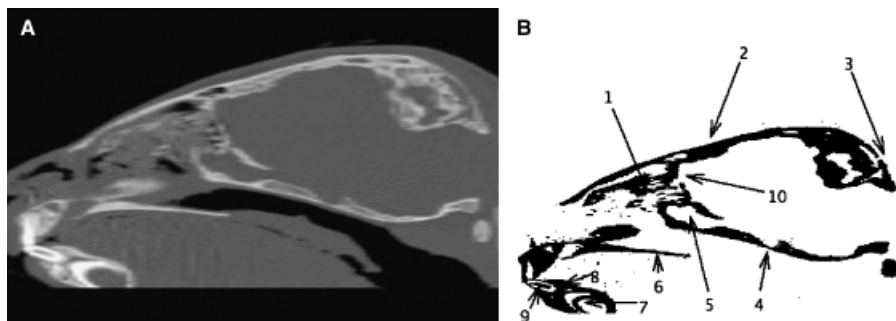


FIG. 1. Sagittal reconstruction just left of midline (1A) and accompanying line drawing (1B). (1) Ethmoid turbinates (ethmoturbinalia), (2) frontal bone (os frontalis), (3) occipital bone (os occipitalis), (4) sella turcica within the basisphenoid bone (os basisphenoidale) containing the pituitary gland (hypophysis), (5) olfactory bulb, (6) hard palate (palatum osseum), (7) left mandibular canine tooth, (8) left mandible (mandibula), (9) left mandibular incisor tooth, (10) cribriform plate (lamina cribrosa).

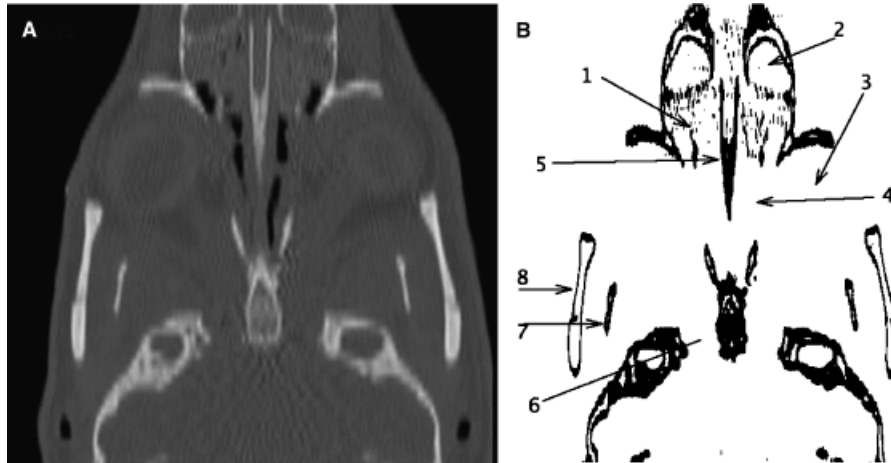


FIG. 2. Dorsal plane reconstruction (2A) and accompanying line drawing (2B). Note the absence of lacrimal bone. Right is to the left of the image. (1) Ethmoid turbinates (ethmoturbinalia), (2) root of left maxillary canine tooth, (3) left eyeball (oculus sinister), (4) absent lacrimal bone (os lacrimale), (5) nasal septum (processus septalis), (6) right optic canal (canalis opticus), (7) right coronoid process of the mandible (mandibula, processus coronoideus), (8) right zygomatic arch (arcus zygomaticus).

bones (identified in domestic species at the ventromedial aspect of the orbit, adjacent to the nasal cavity), and nasolacrimal ducts were not visible.

The mucosal lining of the tympanic bulla was identified as a 2–5-mm-thick soft tissue layer. The tympanic cavities lacked internal septation. The tympanic membrane was only observed in one ear as a very thin film-like structure. The external ear canal was uniformly narrow, measuring approximately 2 mm in diameter.

All teeth were single rooted, and both animals had the same permanent dental formula: I3/2, C1/1, PC6/5 (I, incisor; C, canine; PC, postcanine). In contrast to domesticated mammalian species, the caudal dentition is nondifferentiated in pinnipeds, thus the term *postcanine* is used to identify these teeth.<sup>11</sup>

### Discussion

This study provides detailed information regarding the technical protocol for and the CT anatomy of the California sea lion head. A variety of different technical parameters were used to optimize image quality. Soft tissues were best evaluated using a combination of transverse scanning mode, 2 mm slice width, and a detail image reconstruction algorithm and bone structures best evaluated using a combination of axial scanning mode, 1 mm slice width, and a bone image reconstruction algorithm with additional edge enhancement filter, as expected. Transverse imaging mode is the preferred method for imaging the head due to a full dataset acquired for each image. This is not the situation in helical mode, where missing data have to be interpolated, degrading the final image quality.<sup>12</sup> Image reconstruction

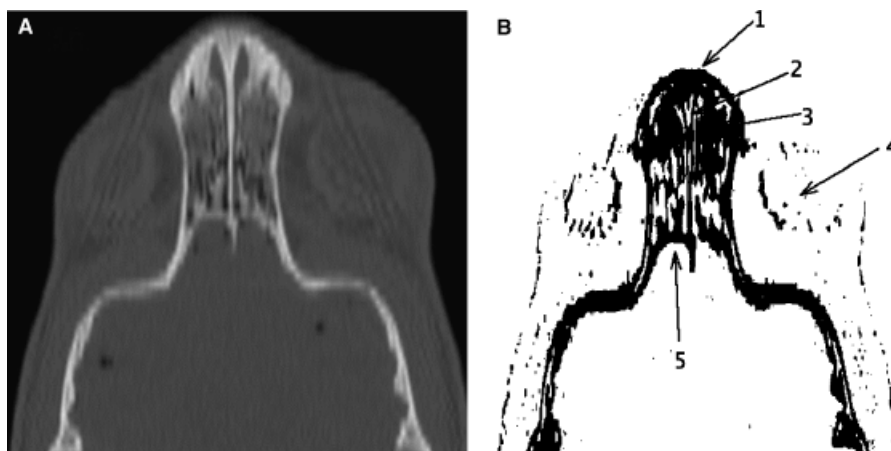


FIG. 3. Dorsal plane reconstruction (3A) and accompanying line drawing (3B). Right is to the left of the image. (1) Incisive/premaxillary bone (os incisivum) containing incisor teeth, (2) ethmoid turbinates (ethmoturbinalia), (3) maxilla, (4) left eyeball (oculus sinister), (5) cribriform plate (lamina cribrosa).

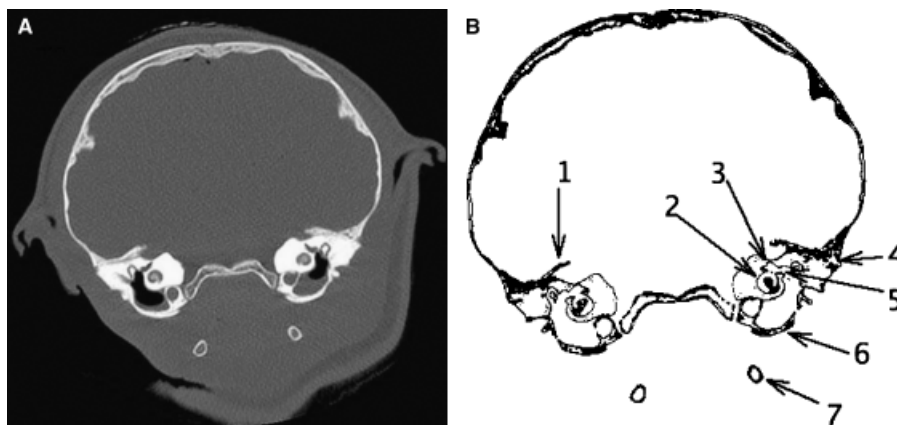


FIG. 4. 1 mm slice thickness transverse CT image (4A), level of the inner ear, and accompanying line drawing (4B). Right is to the left of the image. (1) Cerebellum, tentorium osseum, (2) cochlea (ductus cochlearis) within the petrous temporal bone (os temporale, pars petrosa), (3) internal acoustic meatus, (4) petrous temporal bone (os temporale, pars petrosa), (5) incus, (6) tympanic bulla (bulla tympanica), (7) left stylohyoid bone (os stylohyoideum).

algorithms are weighted Fourier transformations of the image data. Medium-frequency image reconstruction algorithms (General Electric [GE] proprietary term “detail”) will decrease image noise by a smoothing effect, thus increasing the homogeneity of the tissue. This image reconstruction algorithm is most appropriate for soft tissue structures viewed with a narrow window setting. High-frequency image reconstruction algorithms (GE proprietary term “bone”) increase spatial resolution at the expense of increased image noise. This image reconstruction algorithm is most appropriate for bone viewed with a wide window setting that suppresses visible noise.<sup>12</sup> It was interesting to note that despite the use of these appropriate settings, turbinate detail was lost in regions where they were surrounded by fluid. This is most likely as a result of the effect of an increased point spread function due to the

close proximity of structures with close attenuation values resulting in the inappropriate representation of both.<sup>13,14</sup>

Species-specific anatomic features identified were consistent with previous reports. Structural variations of the California sea lion head are not described among gender and age groups with one major exception being the pronounced sagittal ridge in male California sea lions.<sup>11,15</sup> Structural anatomy will not vary between cadaver studies and live patients except in the event of congenital anomaly or disease, thus the data presented here are relevant and applicable to the live sea lion. The overall poor soft tissue differentiation, with the exception of the orbital region, was likely due to marine mammal adipose tissue being laid as a subcutaneous blubber layer, combined with the poor body condition of these cadavers due to malnourishment.<sup>11</sup> An interesting finding that was not expected was the poor

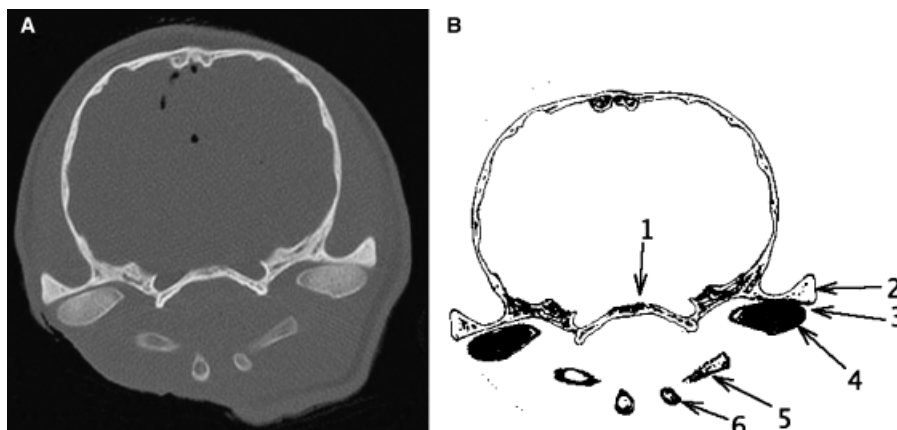


FIG. 5. 1 mm slice thickness transverse CT image (5A), level of the temporomandibular joint (articulatio temporomandibularis), and accompanying line drawing (5B). Right is to the left of the image. (1) Basisphenoid bone (os basisphenoidale), (2) left zygomatic process of the temporal bone (processus zygomaticus), (3) left temporomandibular joint (articulatio temporomandibularis), (4) left condylar process of the mandible (processus condylaris), (5) left ceratohyoid bone (os ceratohyoidum), (6) left stylohyoid bone (os stylohyoideum).

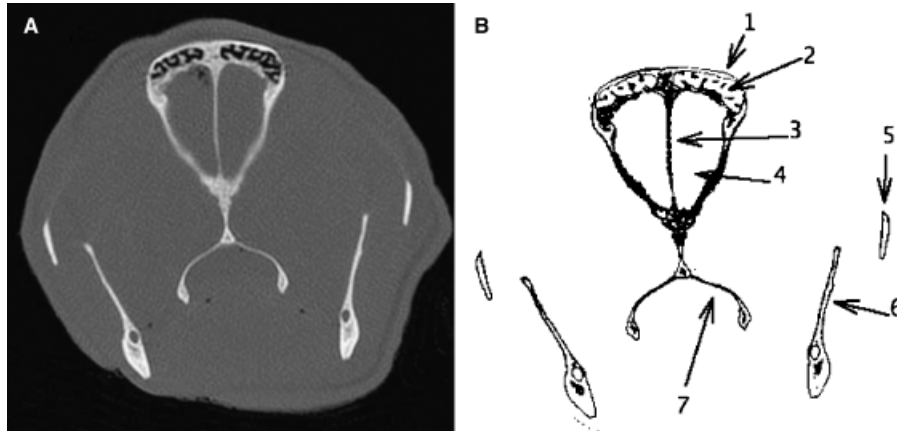


FIG. 6. 2 mm slice thickness transverse CT image (6A), 20 mm rostral to Fig. 5, and accompanying line drawing (6B). Right is to the left of the image. (1) Nasal bone (os nasale), (2) ethmoid turbinates (ethmoturbinalia), (3) ossified septum between the olfactory bulbs (continuation of the perpendicular plate—os ethmoidale, pars lamina perpendicularis), (4) left olfactory bulb, (5) left zygomatic arch (arcus zygomaticus), (6) mandible (mandibula), (7) palatine bone (os palatinum).

definition of oropharyngeal structures. When comparing our images with a published reconstructed sagittal image of a sea lion with a nasal tumor,<sup>6</sup> conspicuity of the tongue and soft palate margins in that image was improved by the passage of an endotracheal tube and surrounding air. Passage of an endotracheal tube was not possible in the cadavers used for this study. However, we anticipate that intubation will permit better evaluation of the pharyngeal area. Severe brain parenchymal degradation was evident grossly, and contributed to the inability to recognize any brain anatomic landmarks, including the ventricular system, in our CT images. This is a limitation of using freeze-thawed cadavers. We anticipate that at least the brain ventricular system will be identifiable in CT images of the live animal, given the different attenuation properties of fluid and brain tissue, but this could not be assessed in our study. The use of contrast-enhanced CT would also be

beneficial for identification of soft tissue changes and vascular anatomy throughout the head.

The thick tympanic cavity mucosa seen during CT imaging of the ear is thought to be an adaptation for diving during which it swells by becoming engorged with blood to decrease the volume of air within the middle ear. Awareness of this normal finding is important to prevent misdiagnosis of ear disease.<sup>8,16</sup>

Deciduous teeth in the *Zalophus* species are shed before birth. All teeth in this study were single rooted with large hypoattenuating pulp cavities, likely due to the young age of the animals.

The fluid identified within the nasal cavity at necropsy and on CT images may have been associated with the nasal mites, the freezing process, the lower respiratory tract disease, or represent normal nasal secretions for the species. The nasal mites embedded in the nasal mucosa that were

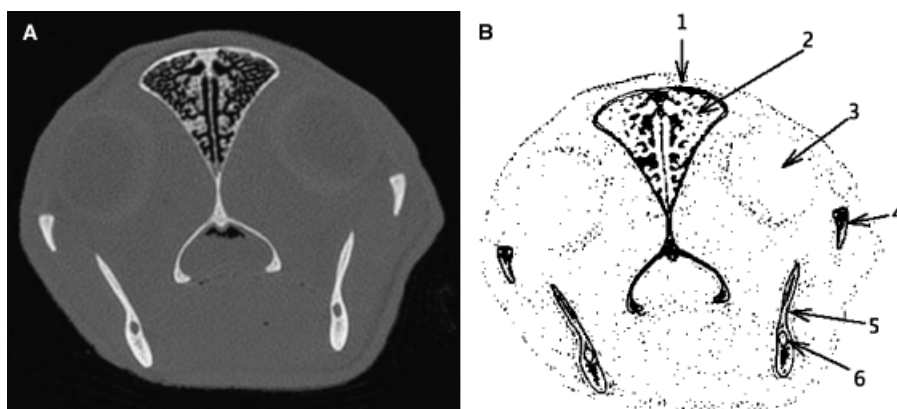


FIG. 7. 2 mm slice thickness transverse CT image (7A), level of caudal postcanine teeth, and accompanying line drawing (7B). Right is to the left of the image. (1) Nasal bone (os nasale), (2) ethmoid turbinates (ethmoturbinalia), (3) left eyeball (oculus sinister), (4) left zygomatic arch (arcus zygomaticus), (5) mandible (mandibula), (6) root of most caudal left postcanine tooth.

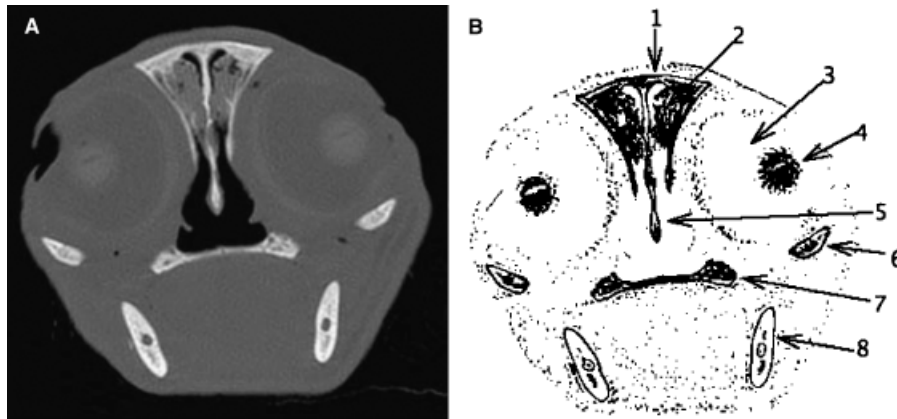


FIG. 8. 2 mm slice thickness transverse CT image (8A), level of mid orbit, and accompanying line drawing (8B). Note the absence of lacrimal bone (os lacrimale) at the ventromedial aspect of the orbit, which is a normal finding in sea lions. Right is to the left of the image. (1) Nasal bone (os nasale), (2) ethmoid turbinates (ethmoturbinalia) surrounded by a small volume of fluid, (3) vitreous humor (corpus vitreum) and posterior chamber of the left eye (bulbus posterior, oculus sinister), (4) lens of the left eye (lens ocularis sinistrae), (5) vomer extending into the nasopharynx, (6) left zygomatic arch (arcus zygomaticus), (7) hard palate (palatum osseum), (8) mandible (mandibula).

identified grossly were not identified on CT images due to their small size and similar attenuating value. The gas within the brain was most likely within peripheral vasculature as a postmortem change.<sup>17</sup>

Free ranging California sea lions that strand due to trauma or human interaction (entanglement, gunshot) affecting the head are not uncommon and require thorough evaluation to determine the extent of the lesion and prognosis for release.<sup>7,9</sup> Otitis has also been recognized.<sup>8</sup> In addition, California sea lions are popular pinnipeds maintained in captivity where interactions within the group or diseases may affect the structures of the head. With extended lifespans associated with captive environments, dental, neoplastic, and other diseases may become increas-

ingly important and advanced diagnostic imaging will be pursued.

The long-term effect of domoic acid toxicosis has recently emerged as an important cause of neurologic dysfunction in free-ranging California sea lions and is important due to the public health concerns. Prognosis for affected animals with intermittent seizures and inappropriate migration patterns is poor and successful release from rehabilitation is unlikely. Uni- or bilateral hippocampal atrophy has been identified on magnetic resonance (MR) imaging of the brain of affected animals.<sup>7,18</sup> It was not possible to identify the hippocampus during this study due to degradation of brain parenchyma. While this warrants further investigation, the utility of CT for assessing

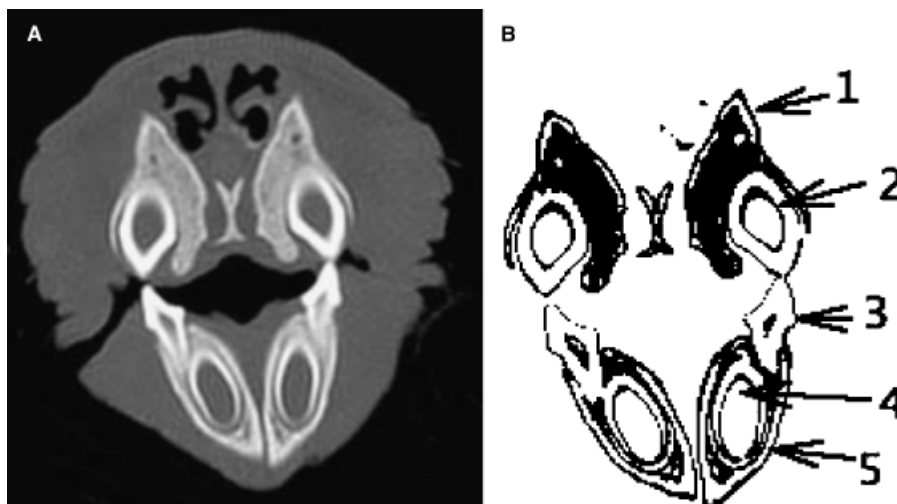


FIG. 9. 2 mm slice thickness transverse CT image (9A), level of the canine teeth, and accompanying line drawing (9B). Right is to the left of the image. (1) Maxilla, (2) left maxillary canine, (3) left mandibular postcanine tooth, (4) left mandibular canine tooth, (5) mandible (mandibula).

the hippocampus is likely to be limited as the hippocampus is in a region often affected by beam-hardening effects.<sup>12</sup> No beam-hardening effects were identified in our two cadavers, but this may have been due to their immature bones and small size compared with adults. In addition, the appropriate window and level required for evaluation of brain will increase image noise. Nevertheless, the exclusion of other causes of neurologic disease including bony trauma, congenital or acquired hydrocephalus or contrast-enhancing lesions of the brain parenchyma such as inflammation or neoplasia should be possible with CT imaging.

This study provides baseline information for the technical imaging protocols and an anatomic description for the head of the immature California sea lion that can be applied to the clinical patient. We recommend the use of 1 mm slice width with a high-frequency image reconstruction algorithm for bone structures and 2 mm slice width with a medium-frequency image reconstruction algorithm for soft tissue structure evaluation. Increases in kVp and mAs may be required for the head of large adult male sea lions to maintain image quality due to the increased head size, bone thickness, and bony sagittal ridge.

#### REFERENCES

- Liste F, Palacio J, Ribe V, et al. Anatomic and computed tomographic atlas of the head of the newborn bottlenose dolphin (*Tursiops truncatus*). *Vet Rad Ultrasound* 2006;47:453-460.
- Morrow KL, Park RD, Spurgeon TL, et al. Computed tomography imaging of the equine head. *Vet Rad Ultrasound* 2000;41:491-497.
- Smallwood JE, Wood BC, Taylor WE, et al. Anatomic reference for computed tomography of the head of the foal. *Vet Rad Ultrasound* 2002;43:99-117.
- George TF, Smallwood JE. Anatomic atlas for computed tomography in the mesaticephalic dog: head and neck. *Vet Rad Ultrasound* 1992;33:217-240.
- Hathcock JT, Pugh DG, Cartee RE, et al. Computed tomography of the llama head: technique and normal anatomy. *Vet Rad Ultrasound* 1995;36:290-296.
- Sherrill J, Peavy GM, Kopit MJ, et al. Use of laser rhinoscopy to treat nasal obstruction in a captive California sea lion (*Zalophus californianus*). *J Zoo Wildl Med* 2004;35:232-241.
- Goldstein T, Johnson SP, Phillips AV, et al. Human-related injuries observed in live stranded pinnipeds along the central California coast 1986-1998. *Aquat Mammals* 1999;25:43-51.
- Gerber JA, Roletto J, Morgan LE, et al. Findings in pinnipeds stranded along the central and northern California coast 1984-1990. *J Wildl Dis* 1993;29:423-433.
- Greig DJ, Gulland FMD, Kreuder C. A decade of live California sea lion (*Zalophus californianus*) strandings along the central California coast: causes and trends, 1991-2000. *Aquat Mammals* 2005;31:40-51.
- Evans HE, deLahunta A. Miller's guide to the dissection of the dog, 3rd ed. Philadelphia: W.B. Saunders Company, 1988;256-274.
- Green RF. Observations on the anatomy of some cetaceans and pinnipeds. In: Ridgway SH (ed): *Mammals of the sea: biology and medicine*. Springfield: Charles C. Thomas Publishing, 1972;247-295.
- Bushberg JT, Seibert JA, Lediholdt Jr. EM, Boone JM. Computed tomography. In: Bushberg JT (ed): *The essentials of medical imaging*. Philadelphia: Lippincott Williams & Wilkins, 2002;355-356, 358-360, 367-372.
- Barthez PY, Koblik PD, Hornof WJ, et al. Apparent wall thickening in fluid filled versus air filled tympanic bulla in computed tomography. *Vet Rad Ultrasound* 1996;37:95-98.
- Auriemma E, Voorhout G, Barthez PY. Determination of optimal window width and level for measurement of the canine pituitary gland height on computed tomographic images using a phantom. *Vet Rad Ultrasound* 2007;48:113-117.
- Nishiwaki M. General biology. In: Ridgway SH (ed): *Mammals of the sea: biology and medicine*. Springfield: Charles C. Thomas Publishing, 1972;136-143.
- Odend'hal S, Poulter TC. Pressure regulation in the middle ear cavity of sea lions: a possible mechanism. *Science* 1966;153:768-769.
- Gan Heng H, Tian Teoh W, Sheikh-Omar AR. Postmortem abdominal radiographic findings in feline cadavers. *Vet Rad Ultrasound* 2008;49:26-29.
- Haulena M, Dold C, Colegrove K, et al. Long term neurologic effects of exposure to domoic acid in stranded California sea lions. *Abstr Proc Am Assoc Zoo Wildl Vet* 2004;227-228.